RPA flight pattern and GCP influence on SfM-MVS modeling of a stable landslide in SE Brazil

Carlos H. Grohmann, Helen Cristina Dias
Institute of Energy and Environment, Universidade de São Paulo, São Paulo, Brazil
guano@usp.br, helen.dias@usp.br

Guilherme P.B. Garcia, Camila Duelis Viana, Rebeca Durço Coelho
Institute of Geosciences, Universidade de São Paulo, São Paulo, Brazil
guilherme.pereira.garcia@usp.br, camila.viana@usp.br, rebeca.coelho@usp.br

Abstract—**In this article, we analyze how the flight paths of RPA surveys and the presence/absence of Ground Control Points (GCPs) will impact the surface reconstruction of a stable landslide in southeastern Brazil. We compare the SfM-MVS results from two surveys (2019/2021) in terms of their completeness, georeferencing, and morphometry. The 2019 flight consist of a simple grid pattern, without precise geometric control given by GCPs. In the 2021 campaign, four flight patterns (two simple grids and two cross-grids) were deployed. The data were processed as the individual flights as well as a combination of the two simple grids and two cross-grids. The combination of the simple grids resulted in the most complete DSM, at the expense of a larger processing time. The DSM from the combined cross-grids had fewer voids than those from the simple grids, but with the downside of requiring two flights and longer processing time. Our results indicate that one simple grid flight will be enough to produce a good reconstruction of the surface, with a short processing time.**

I. Introduction

Remotely Piloted Aircrafts (RPAs), or simply “drones”, are essential tools to acquire high-resolution geospatial data in various scientific fields. RPAs offer an easy-to-use, low-cost, and off-the-shelf solution to capture aerial imagery, geophysical data, or collect samples, depending on the payload carried by these platforms.

Digital imagery collected by RPAs can be used to generate high-resolution (i.e., centimeter-level) Digital Elevation Models (DEMs) using Structure from Motion-Multi View Stereo (SfM-MVS) algorithms [1]. Given that the majority of cameras onboard RPAs operate on the visible and near-infrared spectrum, the SfM-MVS process will produce a Digital Surface Model (DSM), that is, a surface that represents the top of canopy and man-made structures [2].

In this article, we analyze how the flight paths of RPA surveys and the presence/absence of Ground Control Points (GCPs) will impact the surface reconstruction of a stable landslide in southeastern Brazil. We compare the SfM-MVS results from two surveys campaigns in terms of their completeness, georeferencing, and morphometry. Based on the results, we discuss their implications in terms of different scenarios, such as multi-temporal monitoring or situations of rapid response to landslide events.

II. Study Area

The area selected is located in the Town of São Sebastião, São Paulo State, southeastern Brazil. It consists of a hillslope vegetated by tall grass with a shallow landslide measuring approximately 250x100m (Fig. 1). Historical satellite imagery shows that the first ruptures of the landslide occurred around 2002 (Fig. 1A).

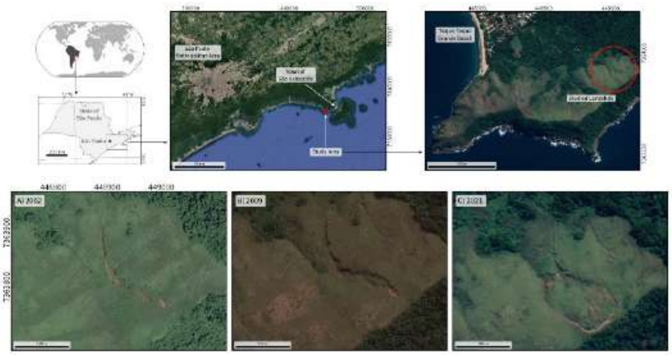

Figure 1. Location of the study area in southeastern Brazil and historical satellite imagery showing the development of the studied landslide.

III. Methods

Fieldwork for the RPA surveys was carried out in October 2019 and May 2021. Images were acquired by a DJI Phantom 4 Pro V2 RPA, carrying a 1″ CMOS 20MP sensor, with global shutter and 8.8 mm focal distance (24 mm at 35 mm equivalent). Flight missions were planned and executed with the MapPilotPro app (https://www.mapsmadeeasy.com/) using the “Terrain Aware” option to plan flights with constant height above ground, providing a constant Ground Sampling Distance (GSD) throughout the study area, regardless of elevation differences. The flight height is based on an SRTM DEM [3].

The 2019 campaign had a reconnaissance objective, so the RPA flights were performed without deploying targets to be used as GCPs. Two missions were flown (Flight #1 - Fig. 2B) with height above ground of 100 m, 70% overlap along and across-track, and camera positioned at -85º.

https://doi.org/10.5281/zenodo.7779223

In the 2021 campaign, nine targets were positioned around the landslide area (Fig. 2A) and their coordinates were determined using a Spectra Precision SP60 DGPS in a base-rover static configuration and raw data was post-processed in Survey Office 4.10 software, using the Ubatuba Station of the Brazilian GNSS Network as reference.

The 2021 flight missions were planned to allow a comparison of different flight patterns in the 3D reconstruction. Two simple patterns were flown with height above ground of 100 m, 80% overlap along and across-track, and camera positioned at -85º (Flights #2 and #3 - Figs. 2C,2D). Two “cross-grid” patterns were flown with height above ground of 120 m, 70% overlap along and across-track, and camera positioned at -85º (Flights #4 and #5 - Figs. 2E,2F). Each flight was processed individually as well as the combination of flights #2+#3 and #4+#5.

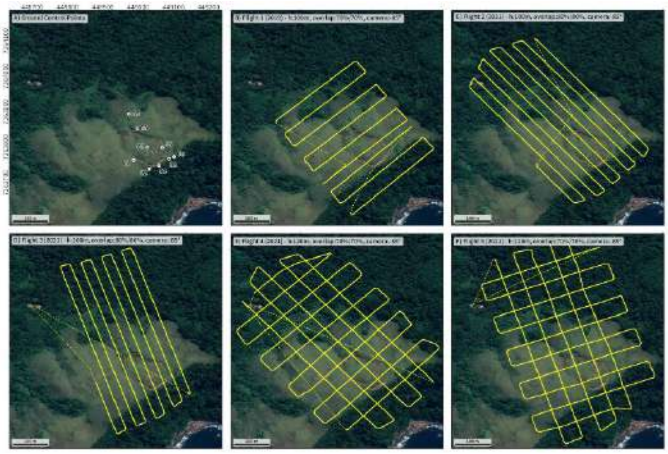

Figure 2. A) Ground Control Points used for georeferencing the SfM-MVS reconstructions. B-F) Flight missions of the RPA surveys. Dashed lines indicate the RPA path to and from the takeoff point.

The combination of flight lines with different orientations is recommended to mitigate distortions from the camera’s self-calibration [4], while the combination of cross-grid patterns with lower overlap intents to simulate the amount of overlap of the simple pattern flights, but with flight plans that are faster to execute [5].

The SfM-MVS workflow was processed in Agisoft Metashape Pro version 1.7.1 (https://www.agisoft.com). In the SfM step, images were aligned with ‘High’ accuracy. Camera alignment optimization was performed considering a marker accuracy of 0.005 m. The MVS step was set to ‘High’ quality and ‘Moderate’ depth filtering.

To evaluate the ‘completeness’ of the reconstructions, the point clouds were imported into GRASS-GIS using the r.in.xyz module as rasters with 10 cm resolution. We set a mask to limit the analysis to the mid and upper portion of the landslide and counted the number of empty (void) pixels.

The subsequent analyses were run using DSMs with 25 cm resolution. The point clouds were imported using the r.in.xyz module, and the voids were filled with bilinear splines. We evaluated the descriptive statistics of each DSM as well as topographic profiles and surface roughness, calculated as the standard deviation of slope [6] using moving-windows with 3x3 pixels.

IV. Results

Processing of the DGPS data resulted in horizontal precision ranging from 0.003-0.005m and vertical precision between 0.007-0.012m. The characteristics of the point clouds from the SfM-MVS workflow are summarized in Table I, including the processing time and the number of voids (i.e., empty 10 cm pixels). Figure 3 shows the distribution of voids for the 2021 flights (2-5 and combinations).

TABLE I. Characteristics of the point clouds

Flight	Photos	Pts.SfM	Pts.MVS	Proc.Time	Voids
1	90	262,691	62,228,877	00:09:59	17094
2	240	701,467	135,262,726	00:36:47	5206
3	208	585,187	136,205,251	00:29:59	5905
2+3	448	1,285,173	164,681,081	01:33:24	1448
4	157	496,613	103,268,426	00:20:48	13710
5	209	572,845	120,873,488	00:35:41	9220

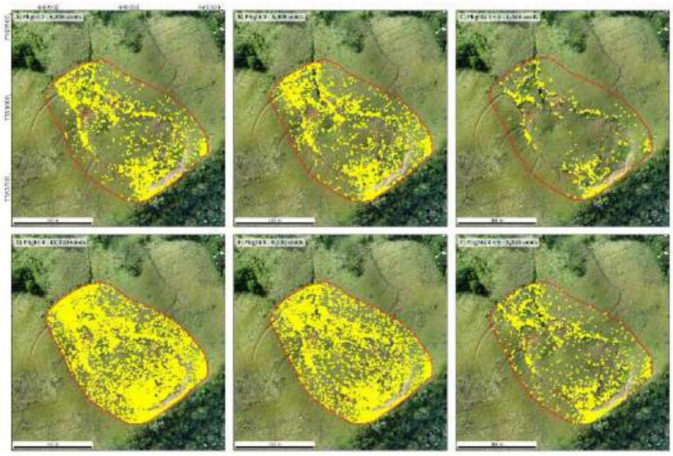

Figure 3. Distribution of voids for the analyzed flight missions. Each dot represents one empty 10 cm pixel.

Processing time varied from ~10’ for flight #1 (2019) to ~30’ for the single and cross-grid flights (2021), up to ~1:30 for the combined flights. The combination of flights resulted in a significant decrease in the number of voids, both for the simple and the cross-grid flight patterns (Figs. 3C and 3F).

The combination of the cross-grid flights #4 and #5 resulted in a dense point cloud with a similar number of points to the simple flights #2 or #3, despite a longer processing time. The combination of simple flights #2 and #3 resulted in ~3-4x fewer voids than in the simple flights, occurring mainly in areas of shadows or dense vegetation.

Five topographic profiles were extracted from the DSMs with 25 cm resolution. The results from the 2021 flights are all very similar, and no visual differences can be identified (solid lines in Fig.4). Profiles from the 2019 flight (dashed lines in Fig.4), in which no GCPs were used, show only a small difference in the horizontal position compared to the 2021 flights. The vertical position, on the other hand, is almost 60 meters lower than its true value.

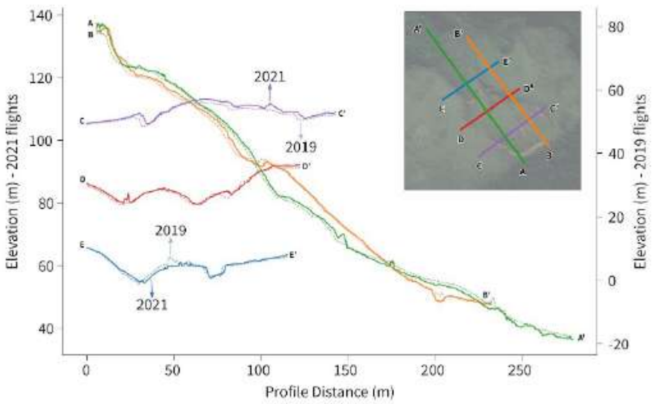

Figure 4. Topographic profiles for the 2019 (dashed lines) and 2021 flights (solid lines).

In the histograms of Fig.5, the curves of the 2021 DSMs overlap almost perfectly, except for the interval between 20 m and 40 m, which corresponds to the densely vegetated area in the NW portion of the surveys. The curve of the 2019 flight shows a similar shape to the 2021 flights, but shifted to the left in the X-axis, as a consequence of the difference of ~60 m in elevation.

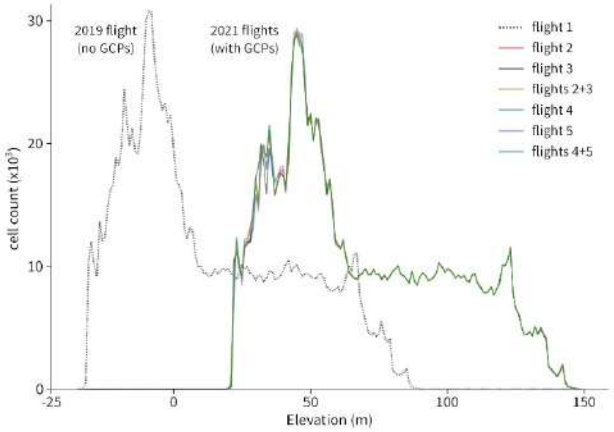

Figure 5. Histograms for the 2019 (dashed line) and 2021 flights (solid lines).

Descriptive statistics of the 25 cm-resolution DSMs are presented in Table II. All DSMs from the 2021 campaign show similar results, with small differences in the minimum and maximum values.

TABLE II. DESCRIPTIVE STATISTICS OF THE DSMS

Flight	min	max	mean	median	std. dev.
1	-35.076	89.981	13.157	3.541	30.311
2	19.877	149.344	68.423	58.758	31.537
3	19.859	147.865	68.413	58.774	31.545
2+3	19.860	148.002	68.387	58.749	31.562
4	20.516	146.984	68.506	58.809	31.456
5	19.514	148.130	68.487	58.806	31.462
4+5	19.127	148.130	68.392	58.741	31.549

V. DISCUSSIONS AND CONCLUSIONS

Visually, all the resulting DSMs are similar. Processing time was around 20-30' for the simple and cross-grids, and 1:30' for the combinations. The DSMs from the simple grid flights had fewer voids than any of the cross-grid flights. The combination of the simple grids resulted in the most complete DSM, at the expense of a larger processing time. The intention of combining cross-grid flights was to simulate the amount of overlap of the simple grid flights. Indeed, the DSM from the combined cross-grids had fewer voids than those from the simple grids, but with the downside of requiring two flights and longer processing time.

Topographic profiles extracted from the DSMs of 2021 are virtually indistinguishable one from another, confirming that the flight patterns did not influence the surface reconstruction. Profiles from the 2019 DSM show small differences in shape that can be attributed to changes in the tall grass vegetation covering the hillside. The main difference is with respect to the Z-axis, where the 2019 DSM is about 60m lower than the 2021 DSMs.

The presence of vegetation cannot be dismissed when interpreting these data, as the SfM-MVS process will generate a DSM and not a DTM. If the area of interest is covered by dense vegetation, one must consider the use of lidar, as the multiple returns of the laser pulse (in the case of airborne lidar) or the very high density of points/m2 (in the case of RPA-borne lidar), allow the removal of vegetation and creation of a "bare earth" surface.

In situations of rapid response to landslide events, time is of utmost importance. Our results indicate that one simple grid flight will be enough to produce a good reconstruction of the surface, with a short processing time. In such situations, deploying GCPs and collecting coordinates with DGPS might also not be a feasible task (both in terms of time, accessibility, and safety).

We show that the DSM produced without GCPs had little difference in the XY coordinates from those where GCPs were applied; the main difference was in the Z-axis, which can be easily adjusted in a GIS environment based on other data (such as previous DSMs/DTMs or topographic maps). In this case, it is important to plan the flights to cover a larger area, to capture features that can be used in the georeferencing, and to set the camera position to off-nadir (85º is sufficient), to prevent dome-shaped distortions in the results. Mapping a larger area also allows for monitoring the landslide without GCPs, since point clouds or DSMs from different dates can be aligned based on their stable features.

Given that landslides usually occur in areas of high relief, the flight plans should consider the terrain and be executed with constant height above ground, to provide a consistent pixel size across the region.

VI. ACKNOWLEDGMENTS

This project was supported by FAPESP (grants #2016/06628-0, #2019/26568-0) and CNPq (grant #311209/2021-1). G.P.B.G. and R.D.C. are PhD students financed by CAPES Brasil (Finance Code 001). H.C.D. is a PhD student financed by FAPESP (grant #2019/17261-8).

REFERENCES

[1] Carrivick, J. L., Smith, M. W., & Quincey, D. J., 2016. Structure from Motion in the Geosciences. In: Analytical Methods in Earth and Environmental Science. Wiley.

[2] Guth, P.L., Niekerk, A.V., Grohmann, C.H., Muller, J.-P., Hawker, L., Florinsky, I.V., Gesch, D., Reuter, H.I., Herrera-Cruz, V., Riazanoff, S., Lópéz-Vázquez, C., Carabajal, C.C., Albinet, C., Strobl, P., 2021 - Digital Elevation Models: Terminology and Definitions. Remote Sensing, 13(18):3581. https://doi.org/10.3390/rs13183581

[3] Farr, T. G., Rosen, P. A., Caro, E., Crippen, R., Duren, R., Hensley, S., Kobrick, M., Paller, M., Rodriguez, E., Roth, L., Seal, D., Shaffer, S., Shimada, J., Umland, J., Werner, M., Oskin, M., Burbank, D., & Alsdorf, D., 2007. The Shuttle Radar Topography Mission. Review of Geophysics, 45, RG2004. https://doi.org/10.1029/2005RG000183

[4] James, M. R., & Robson, S., 2014. Mitigating systematic error in topographic models derived from UAV and ground-based image networks. Earth Surface Processes and Landforms, 39(10), 1413–1420. https://doi.org/10.1002/esp.3609

[5] OpenDroneMap Community, 2020. OpenDroneMap's documentation. https://docs.opendronemap.org/tutorials.html#calibrating-the-camera

Grohmann, C. H., Smith, M. J., & Riccomini, C., 2011. Multiscale Analysis of Topographic Surface Roughness in the Midland Valley, Scotland. Geoscience and Remote Sensing, IEEE Transactions On, 49(4), 1200–1213. https://doi.org/10.1109/TGRS.2010.2053546